Journal of Power Sources 235 (2013) 54–61

Contents lists available at SciVerse ScienceDirect

Journal of Power Sources

journal homepage: www.elsevier.com/locate/jpowsour

Preparation and high temperature performances of $DyCrO_3$-based coatings on a ferritic stainless steel interconnect material

Z.J. Feng, Y.X. Xu, C.L. Zeng*

State Key Laboratory for Corrosion and Protection, Institute of Metal Research, Chinese Academy of Sciences, 62 Wencui Road, Shenyang 110016, China

HIGHLIGHTS

- ► $DyCrO_3$-based coatings for a type 430 stainless steel interconnect were studied.
- ► A high-energy micro-arc alloying process was employed to deposit $DyCrO_3$ coatings.
- ► The coating inhibits the oxidation of the steel at 850 °C in air and air-10%H_2O.
- ► The coating consists of external $NiFe_2O_4$, middle $DyCrO_3$ and inner Cr_2O_3 layer.
- ► The coating can decrease the area specific electrical resistance of the steel.

ARTICLE INFO

Article history:
Received 6 October 2012
Received in revised form
29 January 2013
Accepted 31 January 2013
Available online 9 February 2013

Keywords:
Solid oxide fuel cell
Metallic interconnect
High-energy micro-arc alloying technique
Dysprosium chromite coating
Oxidation
Area specific resistance

ABSTRACT

The major concerns with the ferritic stainless steel interconnects of solid oxide fuel cells operated at intermediate temperatures are the growth of non-protective oxide scales and the Cr evaporation into the cathode, which can increase significantly the cell resistance and polarization resistance. An additional coating is needed to solve these problems. Perovskite $DyCrO_3$-based coatings for a type 430 stainless steel (430SS) interconnect are prepared by a high-energy micro-arc alloying (HEMAA) process using a rod of $DyCrO_3$-20 wt.%Ni as the deposition electrode. Area specific resistance and oxidation behavior of the uncovered and covered steel at 850 °C in both air and wet air are examined. The as-deposited $DyCrO_3$-based coatings are mainly composed of $DyCrO_3$ with some Ni and (Ni,Fe)Cr_2O_4, with a metallurgical bonding to the substrate. The coated steel in both air and wet air has a relatively fast mass gain in the initial stage, followed by a very low mass gain, forming a three-layered scale with a $NiFe_2O_4$ outer layer, a thick $DyCrO_3$ sublayer and a thin Cr_2O_3-rich inner layer. The $DyCrO_3$-based coatings can inhibit significantly the oxidation of 430SS, especially the breakaway oxidation in wet air, and have a low area specific electrical resistance.

1. Introduction

Solid oxide fuel cells (SOFCs) are a power-generation system that transforms directly chemical energy into electricity through an electrochemical reaction between fuel and oxidant gases [1]. With respect to the conventional electrical production systems SOFCs exhibit the advantages of high efficiency and reduced emissions. Moreover, unlike the lower temperature fuel cells, SOFCs can use a variety of fuels such as hydrogen, carbon monoxide, or even natural gases. Nevertheless, the cost and durability of cell materials are still the key barriers to their commercial applications [2,3]. The reduction of operating temperatures of SOFCs can retard the materials degradation and make it possible to use less expensive materials. For example, high temperature alloys have been considered to replace the brittle and expensive $LaCrO_3$ perovskite as interconnect materials of intermediate temperature SOFCs [4]. Of the commercial high temperature alloys, Cr_2O_3-forming alloys are the leading candidates, among which ferritic stainless steels are the most promising materials for SOFC interconnects. However, the main obstacles to using Cr_2O_3-forming alloys as interconnect materials are their low oxidation resistance and the contamination of the cathode caused by volatile Cr species from the chromia scale [5,6]. To overcome these problems, two ways can be imagined. One way is to develop completely new materials such as Crofer22APU and ZMG232 both of which contain ~22%Cr and form a bi-layered scale composed of external (Mn,Fe)Cr_2O_4 and inner Cr_2O_3 [7–9]. The other way is to apply a coating to protect the metallic interconnects against oxidation while keeping a low area specific

* Corresponding author. Tel.: +86 24 23904553; fax: +86 24 23893624.
E-mail address: clzeng@imr.ac.cn (C.L. Zeng).

0378-7753/$ – see front matter © 2013 Elsevier B.V. All rights reserved.
http://dx.doi.org/10.1016/j.jpowsour.2013.01.192

electrical resistance. Among all the possible coatings, perovskite oxides such as (La,Sr)CrO_3 and (La,Sr)MnO_3 [10–18] and spinel such as $(Mn,Co)_3O_4$ [10,19] coatings are extremely promising due to their high electrical conductivity, thermal compatibility and stability in the oxidizing environments. Some techniques such as sputtering [14], screen-printing [15], sol–gel [16], electrodeposition [17] and plasma spraying [18] have been used to prepare perovskite coatings on stainless steel substrate. In our previous work [20,21], a high energy micro-arc alloying (HEMAA) process has been proposed to deposit $LaCrO_3$-based coatings on ferritic stainless steels. These coatings have a metallurgic bonding to the substrate, and exhibit a good oxidation resistance and a low area specific electrical resistance.

To find an appropriate protective coating for metallic interconnects, it is necessary to balance the oxidation resistance and electrical resistance. Of the oxidation-resistant Al_2O_3, SiO_2 and Cr_2O_3-forming coatings, Al_2O_3 and SiO_2-forming coatings are unsuitable for metallic interconnects due to their poor electrical conductivity, while some Cr-containing oxide coatings such as $LaCrO_3$ have the potential to meet the requirements for oxidation resistance and electrical conductivity. To mitigate the Cr evaporation from $LaCrO_3$, it is of great significance to increase the stability of $LaCrO_3$ and or isolate $LaCrO_3$ from gases. Our previous investigation indicated that the active element dysprosium is more effective in inhibiting the corrosion of Ni than some light active elements such as Y [22]. In this study, it was proposed to replace La by Dy in an attempt to prepare a perovskite $DyCrO_3$ coating using HEMAA.

2. Experimental

2.1. Preparation of $DyCrO_3$ coatings

In this study, a type 430 stainless steel (430SS) was used as substrate alloy. The steel plates were cut into specimens with a size of 10 mm × 15 mm × 1.5 mm, followed by grinding with 150-grit SiC paper and degreasing with acetone.

Fig. 1 gives a schematic diagram for HEMAA process. HEMAA is a micro welding technique using short-duration and high-current electrical pulses to realize the mass transfer from an electrode material (anode) to a metallic substrate (cathode). During HEMAA, a discharging pulse current reaching 10^5–10^6 A cm^{-2} is generated in a small area where the anode and cathode come in contact. The current pulse generates a plasma arc for a short time of around 10^{-6}–10^{-5} s, with the maximum arc temperature of 8000–25,000 °C. As a result, metal transfer takes place from the anode tip to the cathode through the liquid. Therefore, HEMAA normally can produce high-quality diffusion coatings at a lower cost, with a minimal thermal distortion or microstructural changes of the substrate due to low energy transfer involved in the HEMAA process.

Before depositing $DyCrO_3$-based coatings, a Cr-alloying treatment was conducted by HEMAA using a Cr electrode rod with a diameter of 4 mm, with a succession of pulse discharge depositing operation under the conditions of middle voltage (60–70 V) and middle frequency (300–400 Hz). Because the solid reaction between Cr_2O_3 and Dy_2O_3 to completely form $DyCrO_3$ occurs at elevated temperatures (>1100 °C) significantly higher than that between Cr_2O_3 and La_2O_3 to form $LaCrO_3$, it is difficult to produce a thermally grown $LaCrO_3$ coating by the deposition of a Dy-Cr alloying layer and subsequent oxidation treatment at 850 °C in air, as reported in Ref. [21]. Therefore, $DyCrO_3$-based coatings were prepared by the direct deposition of a $DyCrO_3$–Ni layer on the alloy surface using HEMAA. The details for preparing $DyCrO_3$ coatings are as follows. Firstly, $DyCrO_3$ powders were prepared by calcining a mixture of Dy_2O_3 and Cr_2O_3 at 1400 °C. Taking into account the good electrical conductivity of NiO at high temperatures, Ni powder as a binder was then added to prepare a complex $DyCrO_3$–20%Ni (in weight percent) electrode which was obtained by mixing $DyCrO_3$ powders with Ni powders, and then hot-pressing at 1400 °C in vacuum. The obtained $DyCrO_3$–Ni sinter was machined into a rod with a diameter of 4 mm used as the electrode for the deposition of $DyCrO_3$-based coatings. The operation parameters for depositing $DyCrO_3$-based coatings are low voltage (~40 V) and middle frequency (300–400 Hz). All depositions were made in a manual mode, and a strong jet of argon gas was applied to the substrate area to avoid heating and oxidation during HEMAA.

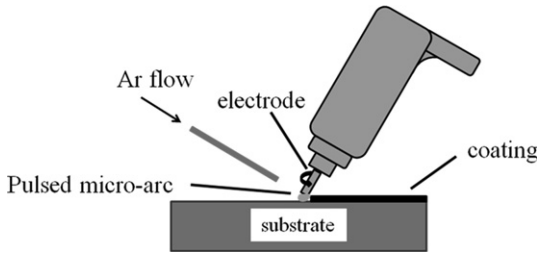

Fig. 1. A schematic diagram for high-energy micro-arc alloying process.

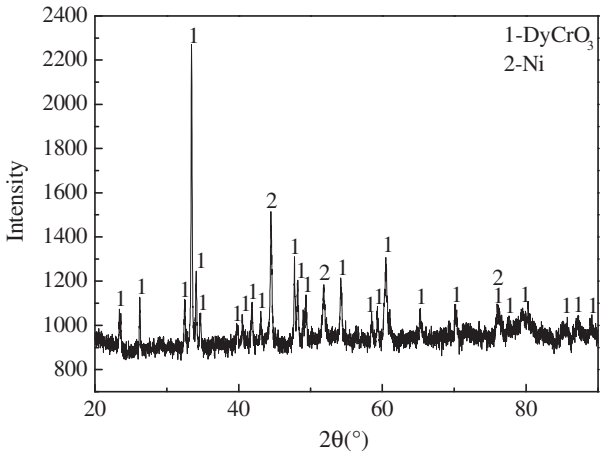

Fig. 2. XRD pattern for the sintered $DyCrO_3$–20%Ni electrode.

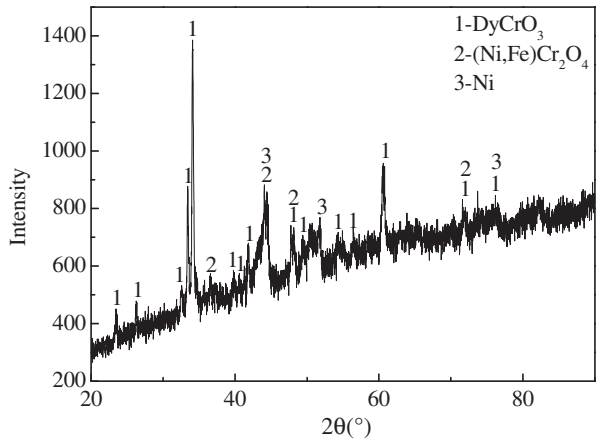

Fig. 3. XRD pattern of the as-deposited $DyCrO_3$ coating on 430SS.

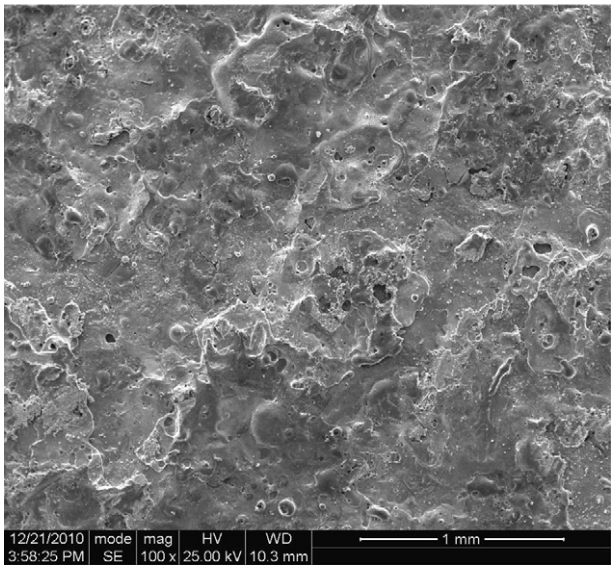

Fig. 4. Surface morphology of the as-deposited $DyCrO_3$ coating on 430SS.

2.2. Oxidation measurements

The oxidation kinetics of the uncoated and coated 430SS was measured at 850 °C in air and wet air containing 10%H_2O, respectively. The air oxidation was conducted in a high temperature furnace. The samples were placed in alumina crucibles, and weighed every 20 h. The wet air oxidation was studied by means of thermogravimetrical balance. Air was allowed to pass through a closed isothermal water box to produce wet air before flowing into the reaction chamber. The temperature of the water box was controlled to be 46 °C corresponding to 10% water vapor. The air flow rate was controlled to be 150 ml min^{-1}. When the furnace was heated to 850 °C, the reaction chamber was purged with wet air for 0.5 h before the specimen was suspended in the reaction chamber for oxidation measurements. The mass change vs. time curves were recorded for a period up to 100 h.

2.3. Area specific electrical resistance measurements

The area specific electrical resistance (ASR) of the uncovered and covered steels was measured using a setup described elsewhere [21]. Platinum paste was applied to the surfaces of the samples pre-oxidized at 850 °C in air for various lengths of time, and then platinum foils were placed on the top of the pastes as current collectors. Pt wires as electric leads were spot-welded to the sides of Pt foils and the resulting resistance was subtracted from the original results. All the electrical resistance measurements were carried out at 850 °C in air.

2.4. Coating characterization

X-ray diffraction (XRD) using PANalytical diffractometer (X'Pertpro) with Cu ka radiation source was employed to characterize the phase formation. The surface and cross-sections of the samples were also examined by scanning electron microscope (SEM) (FEI Inspect FSEM) equipped with an Oxford energy dispersive X-ray (EDX) microanalysis system.

3. Results and discussion

3.1. Characterizations of the as-prepared $DyCrO_3$ coatings

Fig. 2 shows the XRD pattern of the sintered $DyCrO_3$–20%Ni electrode. The electrode is composed of perovskite oxide $DyCrO_3$ and Ni. No new phases are detected. Ni particles as a binder help to increase the electrical conductivity of the electrode at room temperature and decrease its brittleness, thus improving the bonding between the coating and the substrate.

Fig. 3 presents the XRD pattern of the as-deposited $DyCrO_3$-based coating on 430SS. The coating mainly consists of $DyCrO_3$ with some Ni and (Ni,Fe)Cr_2O_4. It is clear that a new (Ni,Fe)Cr_2O_4 phase is generated during the deposition process. During HEMAA, mass transfer occurs between the deposition electrode and the substrate alloy, i.e. $DyCrO_3$ and Ni transfer from the electrode to the alloy surface, and some elements such as Cr and Fe from the substrate alloy to the coating. The new phase (Ni,Fe)Cr_2O_4 results from the reactions among Ni, Fe, Cr and $DyCrO_3$ at high temperatures produced by HEMAA.

The surface morphology of the as-prepared $DyCrO_3$ coating (Fig. 4) shows clearly that the coating exhibits a molten appearance which is the typical characteristics of HEMAA process. During HEMAA, the electrode material is spurted to the surface of 430SS, and some molten drops are deposited jointly.

Fig. 5 shows the cross-sectional morphologies of the as-deposited $DyCrO_3$ coating. The coating presents non-uniform thickness due to manual deposition, with a three-layered

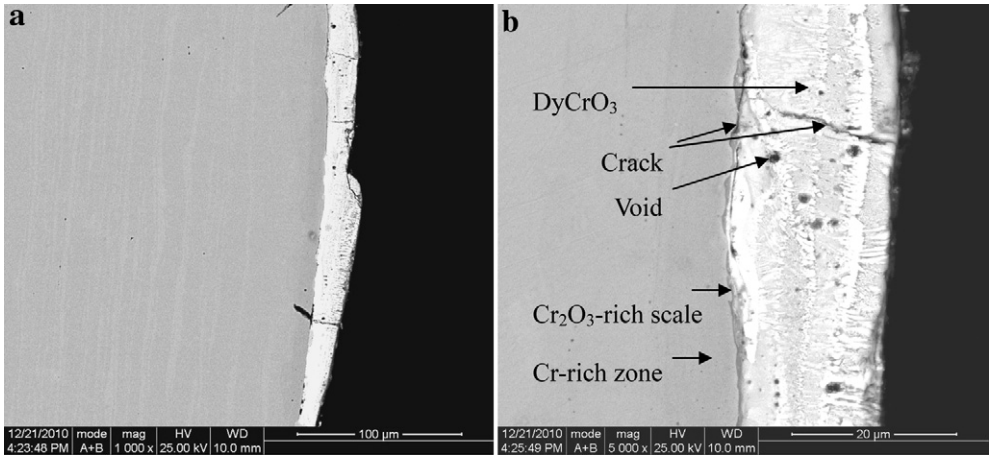

Fig. 5. Cross-sectional morphologies of the as-prepared $DyCrO_3$ coating on 430SS. (a) General view (b) amplified view of (a).

microstructure. The external layer is thick, and mainly composed of bright $DyCrO_3$ incorporating some Cr-rich oxides (gray), beneath which is a very thin Cr_2O_3-rich layer. The innermost layer is a gray Cr-rich alloying layer. Meanwhile, it is observed that some cracks and voids are present in the coating and at the oxide coating/substrate interface.

3.2. Oxidation kinetics

Fig. 6 shows the air oxidation kinetics of the uncovered and covered 430SS at 850 °C. The oxidation of 430SS during the experimental duration of 200 h follows approximately a parabolic rate law, with a low mass gain, while the coated 430SS goes through a fast mass gain in the initial stage, followed by a very low mass gain. The fast mass gain for the coated steel at the initial stage is mainly ascribed to the oxidation of Ni and Fe existing in the as-prepared coating. After the consumption of Ni and Fe in the coating and the formation of a compact oxide layer, the oxidation rate of the coated 430SS is reduced significantly.

Fig. 7 shows the oxidation kinetics of the uncoated and coated 430SS at 850 °C in wet air. The corrosion process of 430SS includes two stages, i.e. an incubation oxidation and a breakaway oxidation stage. In the incubation stage, the steel is corroded slightly, with a low oxidation rate. After oxidation for around 20 h, the steel suffers from a breakaway oxidation, with a significant increase in the mass gain. The occurrence of catastrophic oxidation is ascribed to the fact that the protective scales formed in the initial stage undergo partial failures and along these failure regions, some non-protective scales instead of protective scales are formed. Surface observations confirm that the breakaway oxidation is accompanied with the formation of nodules. It is clear that the presence of 10% H_2O in air accelerates significantly the corrosion of 430SS.

Unlike the bare steel, the oxidation behavior of the coated 430SS in wet air is similar to that in air, and no breakaway oxidation is observed, suggesting that the $DyCrO_3$-based coatings can increase significantly the corrosion resistance of 430SS, and exhibit high stability in wet air.

3.3. Oxidation products

XRD analyses indicate that the $DyCrO_3$-based coatings after oxidation at 850 °C in air and wet air, respectively, are mainly composed of $DyCrO_3$ and $NiFe_2O_4$, as shown in Fig. 8.

Fig. 9 gives the surface morphologies of 430SS after corrosion at 850 °C in air and wet air, respectively. The steel corroded in air forms a uniform scale mainly composed of Cr-rich oxides (Fig. 9a), while in wet air, large amounts of nodules consisting of Fe oxides in addition to a Cr-rich scale are observed (Fig. 9b). Cross-sectional observations show that although a thin Cr-rich scale has formed on 430SS in air, it has extremely poor adhesion to the substrate (Fig. 10a,b). Beneath the scale a Cr-depleted layer is formed. In wet air, however, 430SS goes through non-uniform corrosion (Fig. 10c

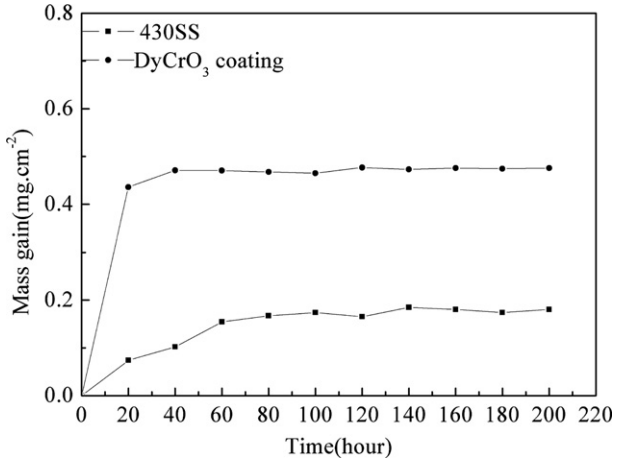

Fig. 6. Oxidation kinetics for the uncoated and $DyCrO_3$-coated 430SS at 850 °C in air.

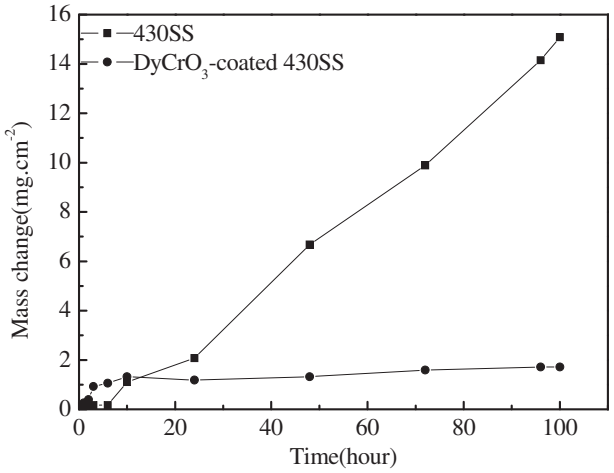

Fig. 7. Oxidation kinetics for the uncoated and $DyCrO_3$-coated 430SS at 850 °C in air–10%H_2O.

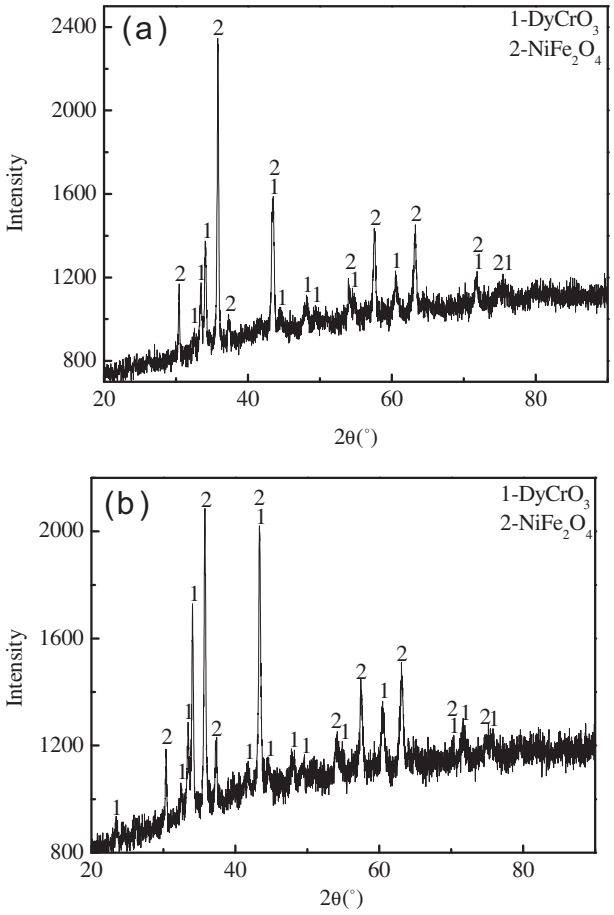

Fig. 8. XRD patterns of the $DyCrO_3$ coatings after oxidation at 850 °C in air for 200 h (a) and in air-10%H_2O for 100 h (b).

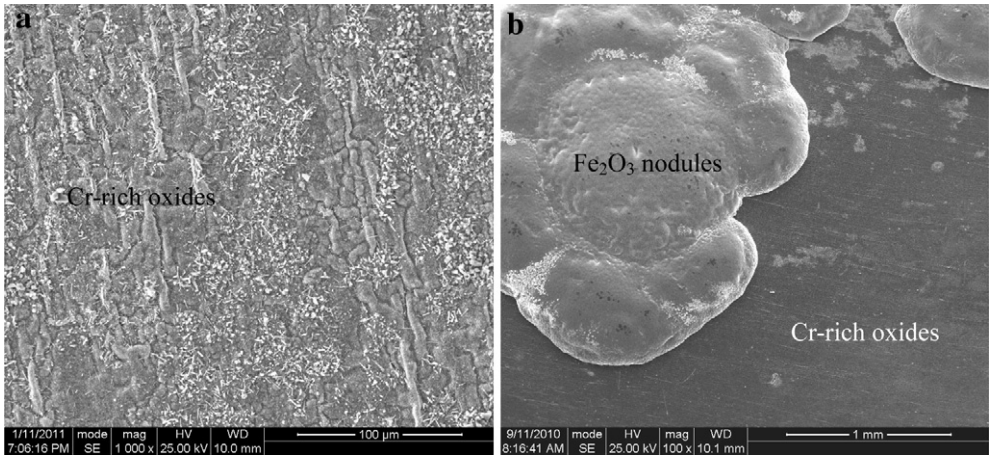

Fig. 9. Surface morphologies of 430SS corroded at 850 °C in air for 200 h (a) and in wet air for 100 h (b).

and d). In the fast corrosion regions, the alloy has formed a thick scale composed of an external Fe oxide (Fe_2O_3) layer and a Fe-rich $(Fe,Cr)_2O_3$ sublayer, while in the areas corroded slightly, a thin Cr-rich $(Cr,Fe)_2O_3$ scale is still observed. The breakaway oxidation of 430SS is clearly related to the formation of nodules.

Fig. 11 presents the surface morphologies of the $DyCrO_3$-coated 430SS after corrosion at 850 °C in air and wet air, respectively. In both environments, the molten appearance of the as-prepared coating is retained to a certain extent. EDX analyses confirm that the external layer of the coatings is mainly composed of Ni and Fe oxides.

The cross-sectional analyses of the coated steel oxidized at 850 °C in air for 200 h show that the coating exhibits a three-layered microstructure with a gray external $NiFe_2O_4$ layer, a thick $DyCrO_3$ sublayer incorporated with some gray Cr-rich oxides, and a thin Cr_2O_3-rich inner layer (Fig. 12). It is noted that some micropores or cracks are present at the substrate/Cr_2O_3-rich layer interface. The Cr_2O_3-rich scale formed along the cracks (Fig. 12b) is

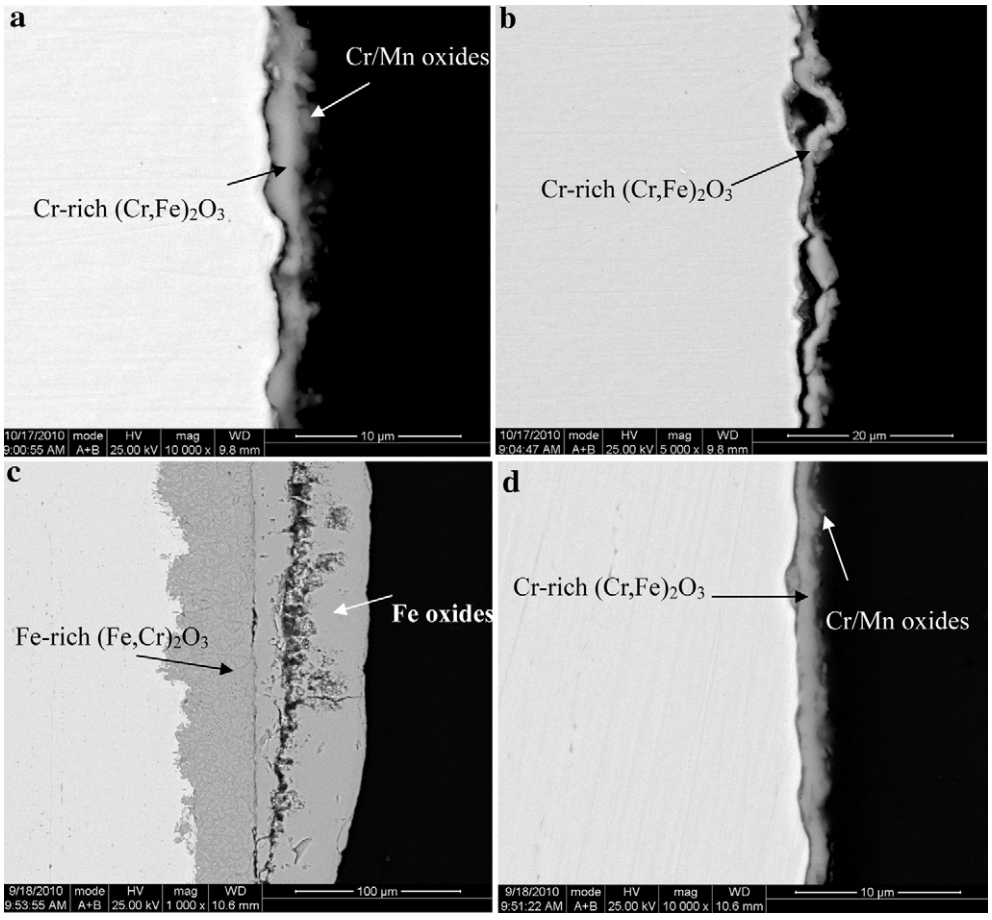

Fig. 10. Cross-sectional morphologies of 430SS after oxidation at 850 °C in air for 200 h (a,b) and in wet air for 100 h (c,d).

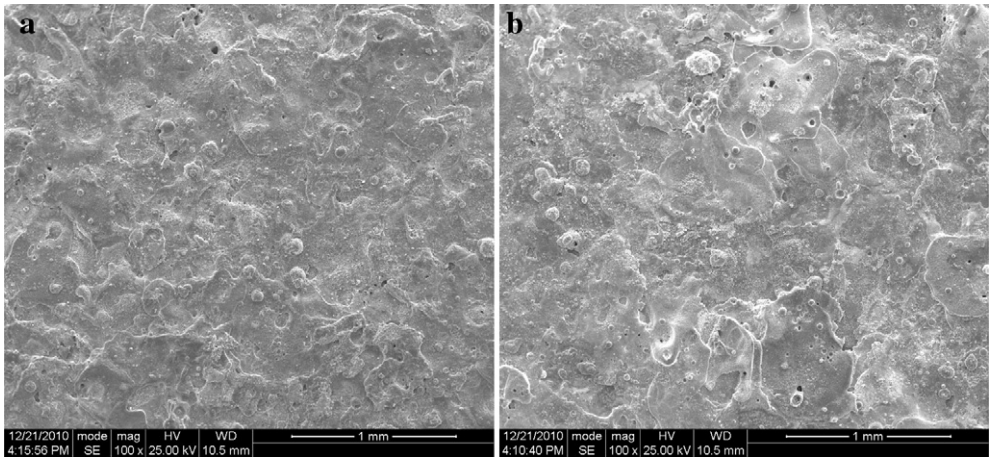

Fig. 11. Surface morphologies of the $DyCrO_3$-coated 430SS after corrosion at 850 °C in air for 200 h (a) and in air-10%H_2O for 100 h (b).

obviously thicker than that along the crack-free regions. These cracks mainly result from the preparation process of the $DyCrO_3$-based coatings. The Cr_2O_3-rich scale along the crack-free interface is very thin and changes little with time. The through-cracks present in the as-prepared coatings have also been filled with Cr-rich oxides. The presence of cracks at the substrate/scale interface is detrimental to the adhesion of the coatings, probably resulting in partial spallation of the coatings. Obviously, more work is still needed to optimize the preparation process of the $DyCrO_3$-based coatings to avoid the generation of cracks. Beneath the oxide layer is a Cr-alloying layer where many gray Cr-rich phases are distributed over the bright substrate alloy. Because Cr in the Cr-alloying layer deposited by HEMAA is in a supersaturated state, Cr-rich phases will precipitate when treated at high temperatures.

The microstructure of the coated steel oxidized at 850 °C in wet air is similar to that corroded in air, as shown in Fig. 13. It should be noted that the manual deposition results in the differences in the thickness of the Cr-alloying layer.

3.4. Area specific electrical resistance

ASR measurements by electrochemical impedance spectroscopy indicate that ASR for the $DyCrO_3$-coated 430SS is increased from around 69–90 mΩ cm^2 after oxidation at 850 °C in air for 50 and 100 h, respectively, while that for the uncovered 430SS oxidized at 850 °C in air for 100 h is around 109mΩ cm^2. The increase of ASR for the coated steel is related to the formation of an outer Ni/Fe complex spinel layer and an inner Cr_2O_3-rich scale, and of cavities along the substrate/scale interface.

3.5. Discussion

The oxidation of 430SS at 850 °C in air follows approximately a parabolic rate law, while in wet air the alloy suffers from breakaway oxidation after an incubation period. The presence of 10% water vapor in air accelerates the corrosion of 430SS. The $DyCrO_3$-based coatings can increase the corrosion resistance of 430SS in air and wet air.

It has been known that water vapor can increase the corrosiveness of environments, and the critical Cr content needed to form a Cr-rich scale in the presence of water vapor is higher than that in the absence of water vapor [23,24]. Several mechanisms including the change of material transport mechanisms in alloy [25], the change of defect-dependent properties of oxide scales due to the incorporation of hydrogen [26,27], and the vaporization of chromia scale from a protective Cr-rich oxide to a less protective $CrO_2(OH)_2$ [28–30] have been proposed to explain the accelerated corrosion caused by water vapor. The re-healing ability of a protective Cr-rich scale depends on the rate of supply of Cr from the alloy to the oxide scale. In the incubation stage, 430SS can form

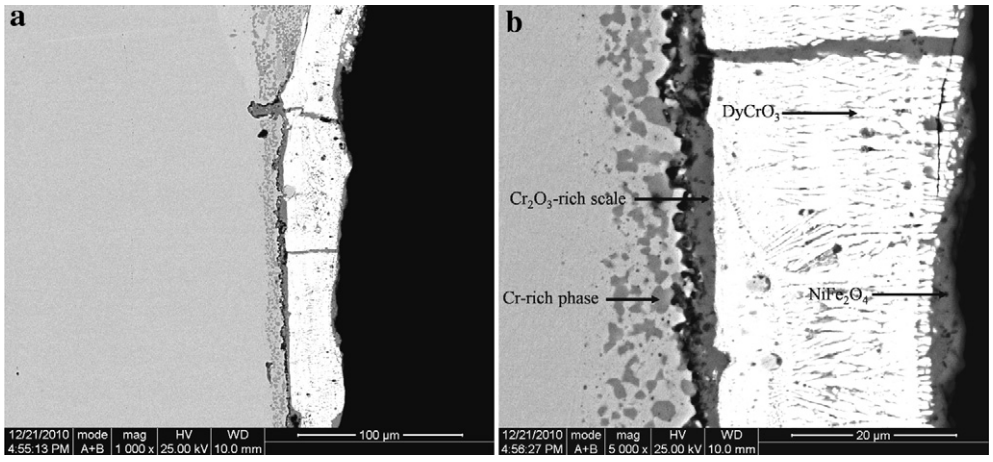

Fig. 12. Cross-sectional morphologies of the $DyCrO_3$-coated 430SS oxidized at 850 °C in air for 200 h. (a) General view; (b) amplified view of (a).

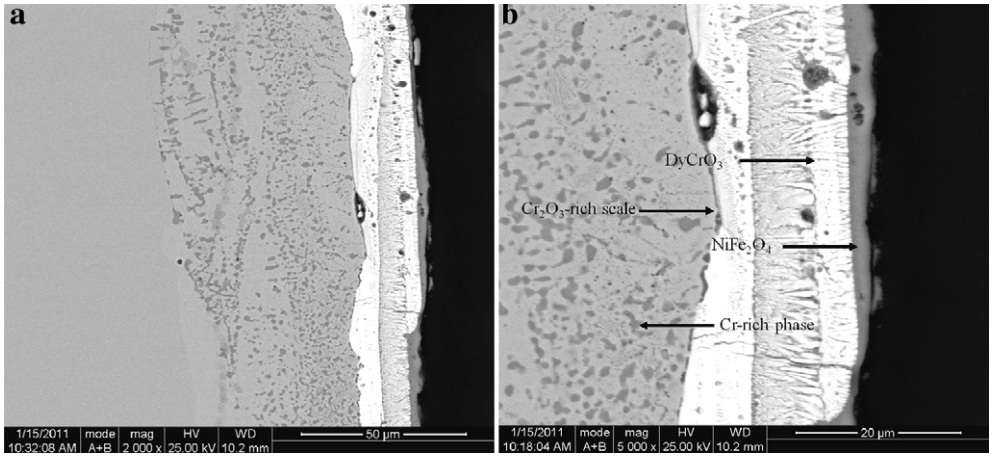

Fig. 13. Cross-sectional morphologies of the $DyCrO_3$-coated 430SS after oxidation at 850 °C in air−10%H_2O for 100 h. (a) General view; (b) amplified view of (a).

a continuous Cr-rich scale beneath which a Cr-depleted zone is produced. Cr can be lost from the protective Cr-rich scale by the following reaction [31]:

$$Cr_2O_3(s) + 2H_2O(g) + 1.5O_2(g) \rightarrow 2CrO_2(OH)_2(g) \quad (1)$$

Cr vaporization from $MnCr_2O_4$ can be expressed by the reaction (2):

$$2MnCr_2O_4(s) + \frac{5}{2}O_2(g) + 3H_2O(g) \rightarrow Mn_2CrO_4(s) + 3CrO_2(OH)_2(g) \quad (2)$$

If the supply of Cr from the alloy to the oxide scale by diffusion is insufficiently rapid to maintain a high Cr concentration in the scale, iron can diffuse easily outward to form nodules of Fe oxides. When the Cr concentration in the Cr-depleted zone is below the critical Cr concentration needed to form a Cr-rich scale, the alloy suffers from fast corrosion. The poor corrosion resistance of 430SS in wet air is mainly ascribed to its low chromium content (17 wt.%) which is insufficient to maintain the growth of a protective Cr_2O_3 scale. Additionally, the poor adhesion of the Cr-rich scales formed on 430SS also shortens the incubation oxidation stage.

When a $DyCrO_3$ coating is applied to the surface of 430SS by HEMAA, the corrosion of the steel, especially in wet air, is inhibited significantly.

As mentioned above, the as-prepared $DyCrO_3$-based coatings are actually composed of $DyCrO_3$ with some metallic particles containing Fe, Cr and Ni etc due to the mass transfer between the deposition electrode and the substrate alloy. When exposed to air and wet air at 850 °C, these metallic particles are oxidized. On one hand, the rapid outward diffusion of Ni and Fe from the coatings gives rise to the formation of a continuous external $NiFe_2O_4$ layer over the $DyCrO_3$ layer, with a fast mass gain as observed. With the consumption of Ni and Fe, the oxidation rate of the covered steel is decreased. On the other hand, the formation of a Cr_2O_3-rich layer at the $DyCrO_3$ layer/substrate interface and Cr-rich oxides inside the $DyCrO_3$ layer helps to increase the protection of the coatings. The protectiveness of the $DyCrO_3$-based coatings is offered by the compact $DyCrO_3$ sub-layer and Cr_2O_3-rich inner layer that act as effective diffusion barriers. It has been shown that $LaCrO_3$ exposed directly to the wet air still releases volatile Cr species, although at a rate three orders of magnitude lower than that for Cr_2O_3(s), leading to an unacceptable degradation in cell performances [31,32]. It is reasonable to consider that the $DyCrO_3$ coatings exposed directly to the wet air can also release volatile Cr species as observed for $LaCrO_3$, although the releasing rate of Cr species is not measured at present. Though the top $NiFe_2O_4$ layer plays a poorer diffusion barrier than both the Cr_2O_3 and $DyCrO_3$ layers, it can isolate the Cr-containing oxides (mainly $DyCrO_3$ and Cr_2O_3) from the wet air, and thus probably help to inhibit the vaporization of Cr from the Cr-containing scales.

Shaigan et al. developed novel and electrodeposited composite Ni−$LaCrO_3$ [17,33] and Co−$LaCrO_3$ [34] coatings for AISI 430 stainless steel, respectively. The oxide scale formed on the surface of the Ni−$LaCrO_3$-coated steel consists of a $LaCrO_3$-filled chromia-rich subscale and an outer layer of Ni−Fe mixed spinel [17,33], while that for the Co−$LaCrO_3$ coated steel is composed of two-layers of cobalt-containing spinel, a Co−Fe spinel as the mid-layer containing $LaCrO_3$ particles and Co_3O_4 as the top layer, and a chromia-rich inner layer also containing $LaCrO_3$ particles [34]. These coatings exhibit a low ASR after oxidation at 800 °C in air, due to the presence of conductive $LaCrO_3$ particles in the chromia-rich subscale, and good adhesion. In the present study, the measured ASR includes the resistance of the scale/coating (Cr_2O_3/$DyCrO_3$/$NiFe_2O_4$) and its interface with the substrate and the Pt electrode. The growth of oxide scales can cause the increase of ASR. The increase of ASR with time for the coated 430SS is related to the growth of external $NiFe_2O_4$ layer and Cr_2O_3-rich inner layer. With the consumption of Ni and Fe etc. existing in the as-prepared coatings and the compactness of the $DyCrO_3$-based coatings, ASR is expected to change little with exposure time. For the uncovered 430SS, however, its ASR increases obviously with time [21]. Although $DyCrO_3$ has a lower electrical conductivity than $LaCrO_3$ [20], it is still effective in inhibiting the oxidation of 430SS, and decreasing its ASR. In the future, the main concern for the $DyCrO_3$-based coatings is how to avoid the generation of voids or cracks along the coating/substrate interface and in the coatings, which is detrimental to the adhesion of the coatings and to the interfacial electrical resistance.

4. Conclusions

A $DyCrO_3$−Ni composite coating has been deposited successfully on the type 430 stainless steel by high-energy micro-arc alloying process using a rod of $LaCrO_3$-20 wt.%Ni as the deposition electrode, with a metallurgical bonding between the coating and the substrate. The as-prepared coatings are mainly composed of $DyCrO_3$ with some Ni and (Ni,Fe)Cr_2O_4. The coated steel undergoes a relatively fast mass gain at the initial oxidation stage at 850 °C in air and wet air, followed by a very low mass gain. After oxidation,

the coatings exhibit a three-layered microstructure composed of an external $NiFe_2O_4$ layer, a thick $LaCrO_3$ middle layer incorporating some small Cr-rich oxides and a thin Cr_2O_3-rich inner layer. The rapid outward diffusion of Fe and Ni existing in the as-deposited coatings to form a $NiFe_2O_4$ top layer is responsible for the fast mass gain in the initial stage. The consumption of Ni and Fe, the formation of a Cr_2O_3-rich scale at the $DyCrO_3$/substrate interface and the compactness of the $DyCrO_3$ coatings give rise to a significant decrease of oxidation rate. The $DyCrO_3$-based coatings can increase significantly the oxidation resistance of 430SS and decrease its ASR. More work is still needed to optimize the deposition parameters to mitigate the generation of voids and cracks along the coating/substrate interface.

Acknowledgments

The project supported by National Natural Science Foundation of China, Grant No 50771101.

References

[1] S.C. Singhal, Solid State Ionics 152-153 (2002) 405–410.
[2] A. Nakajo, F. Mueller, J. Brouwer, J. Van Herle, D. Favrat, J. Power Sources 216 (2012) 434–448.
[3] X.S. Xin, S.R. Wang, J.Q. Qian, C.C. Lin, Z.L. Zhan, T.L. Wen, Int. J. Hydrogen Energy 37 (2012) 471–476.
[4] W.Z. Zhu, S.C. Deevi, Mater. Sci. &Eng. A 348 (2003) 227–243.
[5] S.P.S. Badwal, R. Deller, K. Foger, Y. Ramprakash, J.P. Zhang, Solid State Ionics 99 (1997) 297–310.
[6] Y. Matsuzaki, I. Yasuda, Solid State Ionics 132 (2000) 271–278.
[7] E. Konysheva, U. Seeling, A. Bsemehn, L. Singheiser, K. Hilpert, J. Mater. Sci. 42 (2007) 5778–5784.
[8] P. Huczkowski, N. Christiansen, V. Shemet, J. Piron-Abellan, J. Singheiser, W.J. Quadakkers, Mater. Corros 55 (2004) 825–830.
[9] Y.N. Cheng, C.L. Chu, S. Lee, Corros. Eng. Sci. Technol. 47 (2012) 25–30.
[10] S. Linderoth, Surf. Coat. Technol. 80 (1996) 185.
[11] C. Johnson, R. Gemmen, N. Orlovskaya, Composite B 35 (2004) 167–172.
[12] Y.D. Zhen, S.P. Jiang, S. Zhang, V. tan, J. Eur. Ceram. Soc. 26 (2006) 3253–3264.
[13] C. Johnson, N. Orlovskaya, A. Coratolo, C. Cross, J.W. Wu, R. Germmen, X.B. Liu, Int. J. Hydrogen Energy 34 (2009) 2408–2415.
[14] Z. Yang, G. Xia, G.D. Maupin, J.W. Stevenson, J. Electrochem. Soc. 153 (2006) A 1852.
[15] T. Brylewski, K. Przybylski, J. Morgiel, Mater. Chem. Phys. 81 (2003) 434.
[16] J.H. Zhu, Y. Zhang, A. Basu, Z.G. Lu, M. Parathaman, D.F. Lee, E.A. Payzant, Surf. Coat. Technol. 177 (2004) 65.
[17] N. Shaigan, D.G. Ivey, W. Chen, J. Electrochem. Soc. 155 (2008) D 278–D284.
[18] H.W. Nie, T.L. Wen, H.Y. Hu, Mater. Res. Bull. 38 (2003) 1531.
[19] J.W. Wu, C.D. Johnson, R.S. Germmen, X.B. Liu, J. Power Sources 189 (2009) 1106–1113.
[20] Z.J. Feng, C.L. Zeng, J. Power Sources 195 (2010) 4242–4246.
[21] Z.J. Feng, C.L. Zeng, J. Power Sources 195 (2010) 7370–7374.
[22] Z.P. Liu, P.Y. Guo, C.L. Zeng, J. Power Sources 166 (2007) 348–353.
[23] P. Kofstad, High Temperature Corrosion, Elsevier Applied Science Publishers Ltd, London and New York, 1988.
[24] C.T. Fujii, R.A. Meussner, J. Electrochem. Soc. 111 (1964) 1215.
[25] M. Thiele, H. Teichmann, W. Schwarz, W.J. Quadakkers, VGB Kraftwerkstech. 77 (1997) 129.
[26] G. Hultquist, B. Tveten, E. Hornlund, M. Limback, R. Haugsrud, Oxid. Met. 56 (2001) 313.
[27] G. Hultquist, B. Tveten, E. Hornlund, Oxid. Met. 54 (2000) 1.
[28] H. Asteman, K. Segerdahl, J.E. Svensson, L.G. Johansson, Mater. Sci. Forum 369-372 (2001) 277.
[29] F. Liu, J.E. Tang, T. Jonsson, S. Canovic, K. Segerdahl, J.E. Svensson, M. Halvarsson, Oxid. Met. 66 (2006) 295.
[30] D.J. Young, High Temperature Oxidation and Corrosion of Metals, Elsevier, Oxford, 2008, 455–495.
[31] K. Hilpert, D. Das, M. Miller, D.P. Peck, R. Wei, J. Electrochem. Soc 143 (1996) 3624–3647.
[32] C. Gindorf, L. Singheiser, K. Hilpert, Steel Res. 72 (2001) 528–533.
[33] N. Shaigan, D.G. Ivey, W.X. Chen, J. Power Sources 183 (2008) 651–659.
[34] N. Shaigan, D.G. Ivey, W.X. Chen, J. Power Sources 185 (2008) 331–337.